Remote Sensing in Ecology and Conservation
Open Access
ZSL LET'S WORK FOR WILDLIFE

ORIGINAL RESEARCH

UAV-derived estimates of forest structure to inform ponderosa pine forest restoration

Adam Belmonte[1], Temuulen Sankey[1], Joel A. Biederman[2], John Bradford[3], Scott J. Goetz[1], Thomas Kolb[4] & Travis Woolley[5]

[1]School of Informatics, Computing, and Cyber Systems, Northern Arizona University, Flagstaff, Arizona
[2]USDA Agricultural Research Service Southwest Watershed Research Center, Tucson, Arizona
[3]US Geological Survey Southwestern Biological Science Center, Flagstaff, Arizona
[4]School of Forestry, Northern Arizona University, Flagstaff, Arizona
[5]The Nature Conservancy Northern Arizona Program, Flagstaff, Arizona

Keywords
3D vegetation model, high-resolution image, individual tree detection, restoration, structure-from-motion, UAV

Correspondence
Temuulen Sankey, School of Informatics, Computing, and Cyber Systems, 1298 S. Knoles Drive, Flagstaff, AZ 86011.
Tel: +1 928 523 7098; Fax: +1 928 523 0101; E-mail: temuulen.sankey@nau.edu

Editor: Ned Horning
Associate Editor: Stephanie Bohlman

Received: 11 July 2019; Revised: 8 November 2019; Accepted: 12 November 2019

doi: 10.1002/rse2.137

Abstract

Restoring forest ecosystems has become an increasingly high priority for land managers across the American West. Millions of hectares of forest are in need of drastic yet strategic reductions in density (e.g., basal area). Meeting the restoration and management goals requires quantifying metrics of vertical and horizontal forest structure, which has relied upon field-based measurements, manned airborne or satellite remote sensing datasets. We used unmanned aerial vehicle (UAV) image-derived Structure-from-Motion (SfM) models and high-resolution multispectral orthoimagery in this study to quantify vertical and horizontal forest structure at both the fine- (<4 ha) and mid-scales (4–400 ha) across a forest density gradient. We then used these forest structure estimates to assess specific objectives of a forest restoration treatment. At the fine-scale, we found that estimates of individual tree height and canopy diameter were most accurate in low-density conditions, with accuracies degrading significantly in high-density conditions. Mid-scale estimates of canopy cover and forest density followed a similar pattern across the density gradient, demonstrating the effectiveness of UAV image-derived estimates in low- to medium-density conditions as well as the challenges associated with high-density conditions. We found that post-treatment conditions met a majority of the prescription objectives and demonstrate the UAV image application in quantifying changes from a mechanical thinning treatment. We provide a novel approach to forest restoration monitoring using UAV-derived data, one that considers varying density conditions and spatial scales. Future research should consider a more spatially extensive sampling design, including different restoration treatments, as well as experimenting with different combinations of equipment, flight parameters, and data processing workflows.

Introduction

Forests cover roughly 28% (3.7 billion ha) of the land area on Earth and are cornerstone to the functioning of hydrologic, ecological and sociopolitical systems (FAO, 2015). In the American Southwest, specifically Arizona, there are an estimated 7.48 million hectares of forested land containing roughly 3.98 billion live trees (https://www.fia.fs.fed.us/). Across this region, ponderosa pine (*Pinus ponderosa*) forests have undergone significant changes in their structure, composition and ecological functioning since European-American settlement (hereafter pre-settlement) (Cooper 1960; Fulé et al. 1997; Congalton and Green 2008) due to wildfire suppression, selective logging and livestock grazing (Cooper 1960; Altschul et al. 1989). Pre-settlement regional forest conditions were characterized by a mosaic of diversely aged and structured forest patches with large, irregularly shaped interspaces (Cooper 1961; Sánchez Meador and Moore 2011). Their distributions were dependent on

site-specific conditions (Woolsey 1911; Pearson 1923; Cooper 1960, 1961; White 1985; Mast et al. 1999) and the natural variability of vertical and horizontal forest patch structure yielded an ecosystem adapted to and tolerant of frequent (every 2–26 years), low-severity wildfires and other naturally occurring disturbances such as insect and disease outbreaks (Schubert 1974; Dahms and Geils 1997; Fitzgerald 2005; Castello et al. 2006).

The Southwestern ponderosa pine forests are now characterized by extensive closed canopy forests, comprised of trees usually homogeneous in both age and stature with few old-growth trees, and a uniform horizontal spatial distribution at the landscape scale (Moore et al. 2004; Larson and Churchill 2012; Reynolds et al. 2013). The current forest structure and composition have, in turn, altered the historical ecological functioning, health and resilience of the entire ponderosa pine ecosystem (Kolb et al. 1994; Swetnam et al. 1999; Swetnam and Betancourt 2010). These changes to structure have increased and concentrated the amount of ground surface fuels and tree canopy fuels, leading to greater susceptibility to crown fire (Fulé et al. 2004; Reynolds et al. 2013). Reintroducing the 'natural range of variability' and promoting long-term ecological health of the Southwestern ponderosa pine forests are now recognized as important management goals (Allen et al. 2002; Covington & Moore, 2006; Fulé 2008; Landres et al. 1999).

The United States Congress passed the Forest Landscape Restoration Act (FLRA) in 2008–2009 (Fitch et al. 2018; Schultz et al. 2012) and subsequently the Collaborative Forest Landscape Restoration Program (CFLRP) has allowed the United States Department of Agriculture Forest Service (USFS) to establish and fund a number of large-scale forest management programs (Day et al. 2006; Weldon 2014). Given the collaborative foundations of the CFLRP, a diverse group of stakeholders in Arizona including federal, state, non-profit and private entities established the Four Forests Restoration Initiative (4FRI). As one of the first and the largest forest restoration efforts, 4FRI focuses on reducing the risk of catastrophic wildfire, improving and sustaining watershed health, wildlife habitat and biodiversity across the Apache-Sitgreaves, Coconino, Kaibab and Tonto National Forests (http://4fri.org/). Spanning more than 20 years and covering almost a million hectares, 4FRI will design and implement restoration treatments that selectively harvest and thin dense forests via mechanical thinning and reintroduce fire across the treated areas.

Continued monitoring of restoration treatments is critical in supporting adaptive management goals and ensure the long-term success of 4FRI (Williamson et al. 2011; Four Forests Restoration Initiative, 2013; Schultz et al. 2014). More specifically, quantitative data that catalog changes to forest cover and structure are necessary to evaluate the outcome and the success of a restoration treatment. These data allow managers to determine how well a specific treatment prescription is followed and how future treatments should be tailored to meet larger landscape-scale goals. Acquiring this data has traditionally relied on time-intensive and costly field surveys, which provides thorough, fine-scale measurements at the plot level (0.5 ha) (Smith 2002; USGS 2017). However, given the vast extent of the current and planned restoration treatments, remote sensing-based methodologies are needed for their cost-effectiveness and spatial extent coverage. Here, we assess unmanned aerial vehicle (UAV)-derived aerial imagery and Structure-from-Motion (SfM) models in evaluating the effectiveness of a forest restoration treatment.

Quantifying forest biophysical variables

Planning, implementing and evaluating restoration treatments can greatly benefit from quantitative datasets that summarize pre- and post-treatment conditions in a stand or across the landscape, regardless of the forest restoration objective and desired outcomes (Patton 1977; Covington et al. 1997; Mast et al. 1999; Allen et al. 2002; Kalies and Rosenstock 2013; Bottero et al. 2017; Matonis and Binkley 2018). Evaluating individual treatments with accurate, quantitative datasets helps determine their contribution to the larger restoration plan and associated changes to the plan. Commonly used forest mensuration metrics in restoration planning and assessment are individual tree diameters at breast height (DBH), and stand-level estimates of basal area (BA), trees per hectare (TPH), canopy cover (CC), as well as tree patch and interspace size and shape. Tree patches are groups of trees with similar vegetation composition and structure while interspaces are un-treed 'areas not under the vertical projection of the outermost tree canopies' (Reynolds et al. 2013, p. 71). Traditional field-based methods for these variables rely on trained field personnel, specialized measurement devices, and often lengthy site visits to produce detailed stem maps and stand-level summaries that are used for implementing and monitoring treatments. Additionally, quantifying stand-level metrics requires a combination of sample-driven field measurements of individual trees and statistical modeling techniques (Huffman et al. 2001). To facilitate standardization of data collection, the USFS developed the Common Stand Exam (CSE) guideline, which provide a step-by-step field measurement methodology and acceptable accuracy standards for collection of individual tree and plot-level vegetation data. We use the accuracy standards from the CSE Field

Guide for Region 3 (Southwestern Region) as a baseline in evaluating the UAV-derived estimates of forest metrics.

In contrast to the traditional field-based forest mensuration methods, which tend to cover relatively small spatial extents, airborne lidar (light detection and ranging) data are commonly used to capture structural detail at the landscape level (400 + ha) (Næsset 2004; Reutebuch et al. 2005; Hudak et al. 2006). The continued high costs associated with airborne lidar data acquisition make it unattractive for fine- (0–4 ha) and mid-scale (4–400 ha) projects. This has fostered interest in UAV-borne photogrammetric Structure-from-Motion (SfM) modeling as a viable, cost-effective alternative for fine- and mid-scale assessments (Iizuka et al. 2018; Puliti et al. 2015; White et al. 2013; Alonzo et al., 2018; Carr and Slyder 2018; Diaz-Varela et al. 2016). SfM algorithms construct three-dimensional (3D) models with high point densities and include spectral information. When compared to lidar 3D point cloud data, SfM models often provide similar accuracies in estimating individual tree canopy heights, diameter and volumes (Thiel and Schmullius 2016; Wallace et al. 2016; Sankey et al. 2019). However, SfM photogrammetry in forested environments has unique challenges affecting the quality of data products and their overall accuracies are not well quantified across a gradient of forest conditions (Bohlin et al. 2017; Rupnik et al. 2017; Snavely et al. 2006). More specifically, Iglhaut et al. (2019) reported that uniform forest canopy textures and common patterns could hamper the ability of SfM algorithm, which negatively affect the quality of the data products. The untreated, highly dense forests typical of the 4FRI region might present large areas of tree and ground occlusion, which is expected to limit scene reconstruction. Here, we use UAV-borne photogrammetry to examine the structural changes to a high-density forest that underwent a prescribed mechanical thinning restoration treatment. Specifically, we develop a methodology for measuring forest structure at the fine- and mid-scales to quantify the changes resulting from the treatment, and determine whether this methodology is a viable tool for monitoring prescription-based forest restoration treatments.

Our first objective was to assess UAV-derived high-resolution multispectral imagery and SfM models in quantifying forest vertical and horizontal structural elements at the fine-scale (<4 ha) across a gradient of density conditions. We first hypothesized that the UAV-derived estimates of individual tree location, tree height (m) and crown diameter (m) would not differ significantly from corresponding field-based measurements. Specifically, all of the UAV-derived estimates of tree height and crown diameter would fall within the acceptable error rates used in USFS Common Stand Exam (CSE) protocol. Second, we hypothesized that as tree density, measured in trees per hectare (TPH), and canopy cover increased along a density gradient, the accuracy of all UAV-derived individual tree level estimates would significantly decrease.

Our second objective was to evaluate UAV-derived vertical and horizontal forest structural measurements at the mid-scale (4–400 ha); first by quantifying the forest density and structure metrics before and after the mechanical thinning treatment, and then by comparing post-treatment conditions to the restoration prescription guidelines to determine if treatment objectives were met. We hypothesized that the lower, post-treatment forest density would allow accurate estimates of stand-level basal area (BA), canopy cover, and forest patch and interspace metrics. Additionally, that our workflow, when applied to the post-treatment UAV-image derived datasets, would allow forest managers to efficiently assess restoration treatment objectives.

Materials and Methods

Study area and treatment description

Situated on the southern edge of the Colorado Plateau in northern Arizona, the study area is located in the Coconino National Forest, at the base of the San Francisco Peaks, about 6.5 km from the City of Flagstaff (12S 438346 N., 3901732 E. UTM) (Fig. 1A). The study area includes 46 hectares of forested land, ranging in elevation between 2200 and 2270 m above sea level. It is characterized by relatively flat topography bisected by two distinct ephemeral drainages oriented toward the southwest, with slopes of 0–10% across a majority of the study area and slopes up to 25% found in the drainages. The climate is sub-humid and is characterized by distinct seasonal trends including early summer drought, with an average of 560 mm of precipitation (http://www.wrcc.dri.edu) falling half as snow during winter months and half as rain during the mid-summer monsoon season.

The vegetation is characterized by ponderosa pine *Pinus ponderosa*, which dominates both the region and the study area, and includes intermittent Gambel oak *Quercus gambelii* and Rocky Mountain juniper *Juniperus scopulorum*. The understory vegetation is typical of ponderosa pine-dominated forest in the immediate area and mainly consists of Arizona fescue *Festuca arizonica*, mountain muhly *Muhlenbergia montana*, mutton bluegrass *Poa fendleriana*, bottlebrush squirreltail *Elymus elymoides* and Buckbush *Ceanothus fendleri*. The site had been undisturbed since its last naturally occurring fire in 1876, except for selective historical firewood harvesting (Dieterich, 1980). However, the site was subjected to a prescribed fire in 1976 as a part of a study, in which 63%

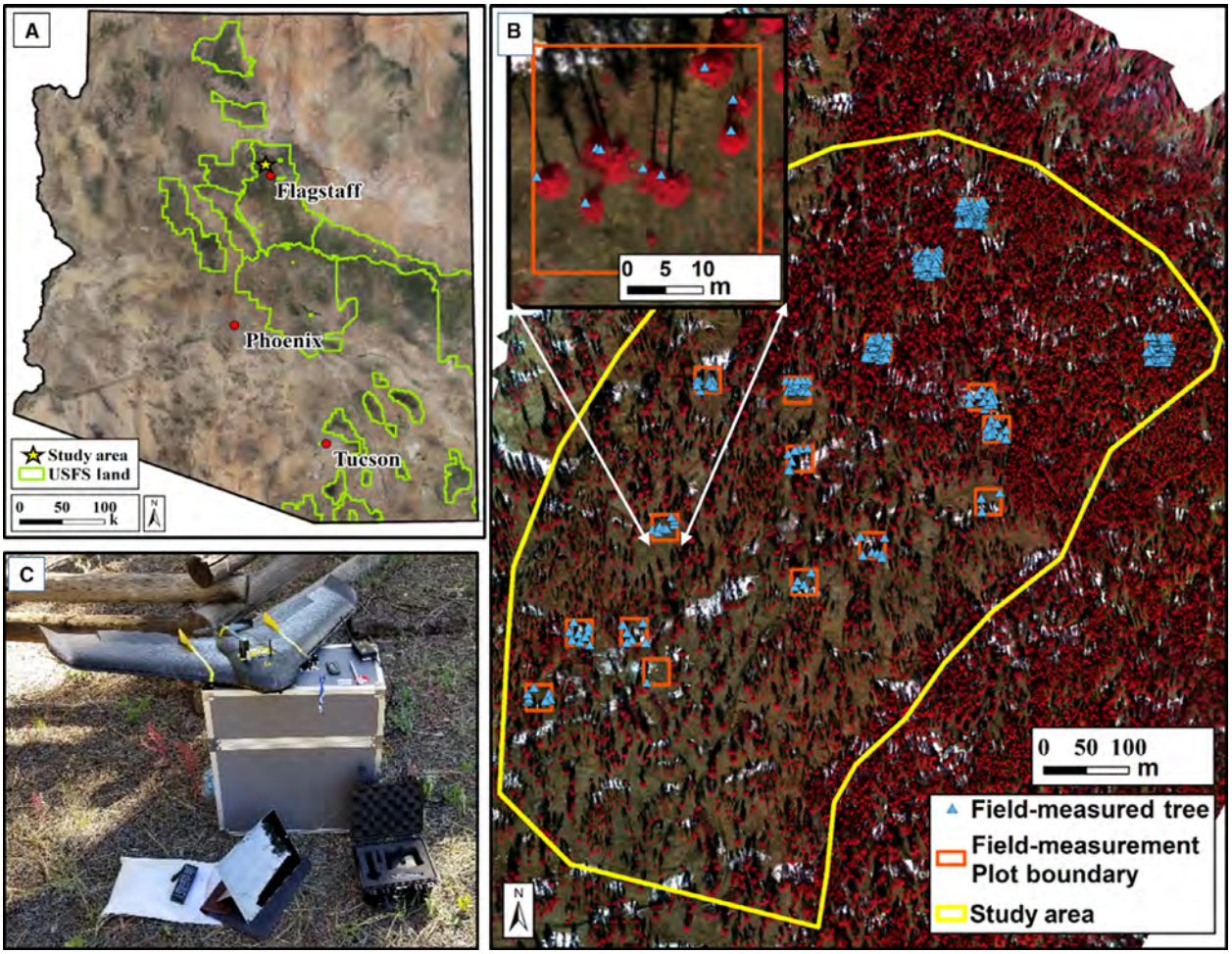

Figure 1. Overview of the study site within the state of Arizona and accompanying US Forest Service land (panel A). The 46.5 ha study area with the field plot locations and an example of a single field plot are shown in panel B, whereas the eBee UAV platform used for all UAV-derived data collection is shown in panel C. Base imagery used in panel B is the post-treatment UAV multispectral orthomosaic image.

of the smaller surface fuels and 69% of the woody surface fuels (up to 8 cm in diameter) were consumed (Sackett, 1979).

Mechanical thinning operations across the study area began during the fall of 2017 and were completed by the spring of 2018. The study area spans two different restoration units and is divided into 30 ha treated and 16 ha untreated areas. Similar to other regional restoration treatments that promote diversity in tree group and interspace size, shape and spacing, this treatment aimed to reinstate pre-settlement forest conditions and included a range of thinning goals that would promote healthy overstory vegetation and the regeneration of understory vegetation (Allen et al. 2002; Larson and Churchill 2012; Reynolds et al. 2013). Specifically, the treatment prescription at our study area emphasized irregular tree group delineation, expansion of interspace, retention of all non-ponderosa pine species (e.g., Gambel oak and juniper) and significant reductions in smaller ponderosa pine trees within groups and interspaces. The treatment was implemented using an approach called designation by prescription (DxP) and digital tree marking, which relied upon outfitting the tree harvesting equipment with tablet computers that use GPS. This supplied the harvesting personnel with location-specific prescription criteria to guide the cutting process. For this study, the same set of GPS-delineated polygons which guided thinning process was used to select for and quantify the patch and interspaces. To assess whether the restoration treatment objectives were met or not, we used estimates of individual tree location and site-wide tree density in TPH and BA.

UAV images and pre-processing

We performed two sets of UAV flights, one before the treatment started (hereafter pre-treatment) during

Table 1. Summary of UAV flight data collection and SfM image reconstruction parameters used in our study, and relevant product characteristics

	Pre-treatment flight	Post-treatment flight
UAV flight information		
Flight date	10/14/2017	1/29/2018
Wind speed	0.61 m/s	0.13 m/s
Cloud cover	0%	0%
Total flight time	1:36:15	1:30:31
Number of images	1285	1369
Total coverage	0.85 km²	1.45 km²
Data processing parameters		
Photo alignment accuracy setting	High	High
Key point limit setting	60,000	60,000
Tie point setting	0 (maximum)	0 (maximum)
Generic pre-selection	No	No
Reference pre-selection	Yes	Yes
Dense cloud quality setting	High	High
Depth filtering setting	Aggressive	Aggressive
Data output details		
Orthomosaic ground resolution	13.6 cm/pixel	15.7 cm/pixel
SfM model tie points	6,496,677	5,406,209
SfM dense cloud points	12,092,123	14,505,513
SfM model reprojection error	0.33 pixel	0.31 pixel
XY error	1.59 m	1.14 m
Z error	1.13 m	1.80 m

October 2017 and another set after the treatment was completed (hereafter post-treatment) during January 2018. We used the Parrot Sequoia multispectral sensor (Parrot Drones SAS, Paris) aboard a Sensefly eBee fixed-wing UAV platform (SenseFly, Lausanne, Switzerland) with a total payload of 690 gr in weight including the platform itself. With a wingspan of 96 cm, it can cover up to 12 km^2 in a single flight (www.sensefly.com/drone/ebee-mapping-drone). All flights were planned and executed using Sensefly's eMotion 3 software (SenseFly, Lausanne, Switzerland), which enabled customized flight plans that controlled all flight and data parameters.

Site-specific characteristics known to cause issues in photogrammetric processing, such as dense forests and heavy shadowing, were carefully considered to ensure consistent data quality within and across flights (Puliti et al. 2015). Specifically, we used perpendicular and interlaced flight lines, high latitudinal and longitudinal overlaps (85% and 90%, respectively), and operated within 60 min of solar noon for all flights. During flight, each photo location included a total of five images; four individual 1.2MP images in the green (530–570 nm), red (640–680 nm), red edge (730–740 nm), and near infrared (770–810 nm) spectral bands, as well as a separate 16MP RGB composite image. Using on-board gyroscopic sensors, each image was assigned a unique set of GPS coordinates (X, Y and Z dimensions) as well as a location relative to the aircraft's principal axes: the *x*-axis (roll), *y*-axis (pitch) and z-axis (yaw). Using the eMotion 3 software, this embedded information along with the flight log was used to geotag and georeference the images for all subsequent processing steps. The resulting pre-treatment dataset consisted of 1285 images per band (6425 total) covering 85 ha and the post-treatment dataset consisted of 1369 images per band (6845 total) covering 130 ha. We performed all flights at a consistent altitude of 122 meters above ground, which resulted in image spatial resolution of 15 cm. Specific flight parameters and environmental conditions are provided in Table 1.

We established ground control points (GCPs) for each flight evenly spread across the study site using a combination of 1 m × 1 m vinyl checkerboard panels and large rocks that would remain visible above the snow in the winter season. Each GCP was mapped using a Trimble GeoXH handheld GPS unit and the data were differentially corrected using GPS Pathfinder Office software. The post-corrected GPS positional accuracies ranged between 0 and 50 cm for 87.5% and 96.5% of the total points for pre- and post-treatment datasets, respectively. Error estimates in the orthomosaic imagery are described in Table 1.

UAV image analysis

Post-processing of individual images into final data products was accomplished using the Agisoft PhotoScan v1.4.0 photogrammetric processing software (Agisoft LLC, St. Petersburg, Russia). In Agisoft, all images from the flights were scanned for matching 'tie-points', oriented in three-dimensional space via bundle-adjustment, and then mosaicked together based on unique overlapping points and spectral similarities (Dandois and Ellis 2013). The general workflow in the software includes image alignment to create a sparse point cloud, incorporation of GCP locations, image alignment optimization, gradual filtering out of inaccurate and error-inducing points, and lastly a full image realignment before data product creation (Puliti et al. 2015; USGS, 2017). Final data products for this study included an undistorted, high-resolution orthomosaic image of the entire study site in 15 cm spatial resolution and four spectral bands, and dense three-dimensional (3D) point cloud data photogrammetrically generated from the high-resolution images using Structure-from-Motion (SfM) algorithms. A full list of parameters used for all image processing steps is provided in Table 1.

Field-based validation dataset

To assess the accuracy of the UAV-derived forest measurements, a total of 17 field plots were established

throughout the study area and were inventoried during the summer of 2018, approximately 5 months after the post-treatment UAV flights. The field plots were each selected to represent a specific forest condition along the canopy cover and stem density gradient, capturing as much variability in forest density across the study area as possible. To assess the effects of forest conditions on UAV image-derived tree measurements, we divided the field-measured plots (n = 17) into groups of varying stem density conditions, which was expressed in trees per hectare (TPH). These density conditions included low (1–89 TPH; n = 5 plots), medium (100–211 TPH; n = 8 plots) and high (467–856 TPH; n = 4 plots). Each plot was 30 m × 30 m in dimension (0.09 ha). Together, the field plots covered roughly 2% (1.53 ha) of the total study area.

Within each plot, the geographic location (X, Y coordinates), height (Z), two canopy widths (widest and narrowest) and the diameter at breast height (DBH) of each tree were measured for all trees taller than 1.37 m. The DBH measurements were used to estimate basal area (BA) at the plot level. Stems less than 1.37 in height were considered as seedlings and not measured due to their low abundance. All trees were stem-mapped using a Trimble Geo7X hand-held GPS unit with the Laser Rangefinder module, with 95.6% of all recorded point locations having <2 m accuracy. A total of 392 individual trees were located and measured across the 17 plots (Fig. 1).

Fine-scale forest structure metrics

Using the UAV image-derived point cloud data, we segmented individual trees and estimated their location (X, Y coordinates), tree height (Z in m), and crown diameter (m). First, the raw SfM point cloud was filtered using the statistical outlier removal tool in CloudCompare software (CloudCompare, 2.9.1, 2018) and then classified into ground versus non-ground points using the Cloth Simulation Filter (CSF) model (Zhang et al., 2016). We performed all steps of the individual tree segmentation (ITS) process using the *lidR* and *rLiDAR* packages (Mohan et al. 2017; Roussel et al. 2017) implemented in RStudio. A digital terrain model (DTM) was produced using the post-treatment classified ground points dataset, which was superior to the pre-treatment dataset due to the greater amount of classified ground points. The overall accuracy of the DTM (R^2 = 0.95, RMSE = 2.98 m) was assessed by comparing points extracted from the DTM to the corresponding points from the differentially corrected GPS elevation values (Z) of the trees in the field-based validation dataset. This DTM was then used to normalize both the pre- and post-treatment point clouds prior to tree segmentation.

Using the ITS algorithm developed by Li et al. (2012), a collection of points was grouped into a tree from the top of the tree crown down using thresholds controlling the relative spacing between trees, the changes in that spacing throughout the height of the tree and the relationship between point distances. The ideal parameters were achieved by iteratively and incrementally testing them with our data and based on the results from previous research (Shin et al. 2018). The final parameters were as follows: distance threshold (DT) 1 of 1.4 m, DT 2 of 1.7 m, minimum height of 2 m, individual point height for triggering DT value of 12 m and the search radius of 0 m. The segmentation and associated tree metric calculation processes yielded a list of all trees segmented with their unique identification number, their geographic coordinates (UTM in meters), heights (m) and two opposing canopy diameters (m).

An accuracy assessment was performed to determine which of the field-measured trees (n = 392) were correctly identified and segmented in the UAV-derived point cloud data. The accuracy assessment consisted of an analysis of omission and commission error rates (Mohan et al. 2017; Shin et al. 2018). The omission and commission analysis quantifies the rate of correctly identified trees or true positive (TP), omitted or false negative (FN) and incorrectly included trees or false-positive (FP) trees. These accuracy categories are summarized by calculating the recall (r), precision (p) and F-score (F) via the following equations:

$$r = \frac{\mathrm{TP}}{\mathrm{TP} + \mathrm{FN}}$$

$$p = \frac{\mathrm{TP}}{\mathrm{TP} + \mathrm{FP}}$$

$$F = 2 \times \frac{(r \times p)}{(r + p)}$$

The correctly identified trees in the UAV image-derived point cloud were then compared to the corresponding trees measured in the field using their height, and crown diameter via paired t tests and simple linear regression models. Differences in individual tree locations were quantified using a simple Euclidean distance from the field-measured GPS tree locations. The UAV image-derived estimates for each variable were also compared to a set of acceptable accuracy ranges utilized by the USFS during their common stand examination (CSE): ±10% for an intensive examination and ±20% for an extensive examination. Analysis of variance (ANOVA) tests with unequal variances were used to compare individual tree metrics among the three density categories: low, medium and high.

Mid-scale forest structure metrics

We estimated stand-level basal area (BA), canopy cover, and forest patch and interspace metrics as well as the changes in these variables resulting from the mechanical thinning treatment. We first established a linear relationship between the field-measured tree density in trees per hectare (TPH) and BA (m^2/ha) at the plot level ($n = 17$) using the following equation:

$$\mathrm{BA}\left(\frac{\mathrm{m}^2}{\mathrm{ha}}\right) = 8.95 + 0.07 * \mathrm{TPH}$$

This relationship yielded R^2 of 0.89 and RMSE of 347 $\frac{m^2}{ha}$, when compared to the field-measured BA. We then extended this relationship to the entire study area using our UAV image-derived tree density estimate from the individual tree segmentation described above to estimate the site-wide BA.

Using the UAV orthomosaic image in the ENVI 5.3 software (Exelis Visual Information Solutions, Boulder, Colorado), we classified canopy cover. The four spectral bands were converted to reflectance and layer stacked together to create a single multispectral image, which was then used to calculate normalized difference vegetation index (NDVI). Using a NDVI value threshold along with a 2-m tree height threshold in the SfM point cloud data, we classified tree canopy versus non-tree canopy cover. Since our study area was dominated by a single, evergreen conifer species, NDVI provided a simple approach in distinguishing tree canopies from the herbaceous understory mixed with some bareground. The integration of the tree height information allowed us to eliminate large piles of cut trees and vegetative material left behind from the mechanical thinning treatment operations. The resulting binary canopy/non-canopy classification was summarized in 10 m cells to estimate total tree canopy cover per cell (in percent). Field-measured canopy cover was calculated by rasterizing each tree's average crown diameter into 15 cm grid cells, then summarizing it into 10 m cells to facilitate direct comparison. The relationship between the field-measured and UAV-derived estimates of canopy cover was assessed using a simple linear regression model. We then quantified the changes in forest canopy cover and BA between the pre- and post-treatment conditions.

Other specific outcomes of the restoration prescription were also quantified using a set forest patch and interspace metrics: patch and interspace shape regularity, size and spacing (Pelz and Dickinson 2014). First, a forest patch and interspace raster was created from the binary canopy cover classification by implementing a clustering algorithm in R-Studio (Girvetz and Greco 2007). The patch summary raster is a binary classification of the pixels labeled by the algorithm as either a forest patch or non-patch (i.e., interspace). This was resampled to 5 m pixels and then used with the FragStats software (McGarigal et al. 2012) to estimate the following specific patch-level metrics: patch area (ha), patch perimeter (m), contiguity index (unitless) and Euclidean nearest random point distance (ENRPD) (m). The contiguity index quantifies the shape of a patch by measuring its contiguity of cells within a 3 × 3 cell neighborhood (McGarigal et al. 2012), whereas ENRPD quantifies the prevalence and size of gaps (Pelz and Dickinson 2014). We summarized the patch-level metrics in both the pre- and post-treatment images and compared them to evaluate the restoration treatment.

Results

Fine-scale forest structure metrics

Our field plots included a total of 392 trees: the low-density plots ($n = 7$) contained 37 field-measured trees, the medium-density plots ($n = 6$) contained 75 trees and the high-density plots ($n = 4$) contained 280 trees. These field-measured trees were used for the assessment of fine-scale, individual-tree metrics derived from the SfM point cloud data (Fig. 2). Overall, 64% of all the trees were correctly identified and segmented in the UAV SfM point cloud data: 92% from low-density, 71% from medium-density and 30% from high-density plots (Table 2). We compared Euclidean distances between tree X and Y coordinates across density classes. ANOVA results indicated there was a significant difference between the classes ($P < 0.01$) and the low- and high-density classes were significantly different.

A simple linear regression model of all individual tree heights showed moderate overall agreement between field-based measurements and UAV image-derived estimates (Fig. 3). Furthermore, a paired t test indicated no significant overall difference ($P = 0.51$) between the field-based measurements ($M = 17.52$ m; SD = 4.58 m) and UAV image-derived estimates ($M = 17.39$ m; SD = 4.65 m). In contrast, comparison of all individual tree crown diameters showed a significant difference ($P < 0.01$) between the field-based measurements ($M = 4.48$ m; SD = 1.66 m) and UAV image-derived estimates ($M = 5.96$ m; SD = 2.46 m). The UAV image-derived crown diameters tended to be overestimated. When we compared the UAV image-derived estimates to USFS Common Stand Exam (CSE) acceptable error rates, 86% of the overall tree height estimations fell within the ±20% range and 63% fell within the ±10% range (Table 3). However, only 29% of the UAV image-derived tree crown diameter estimates was within the ±20% range (Table 3). Both the UAV image-derived individual tree

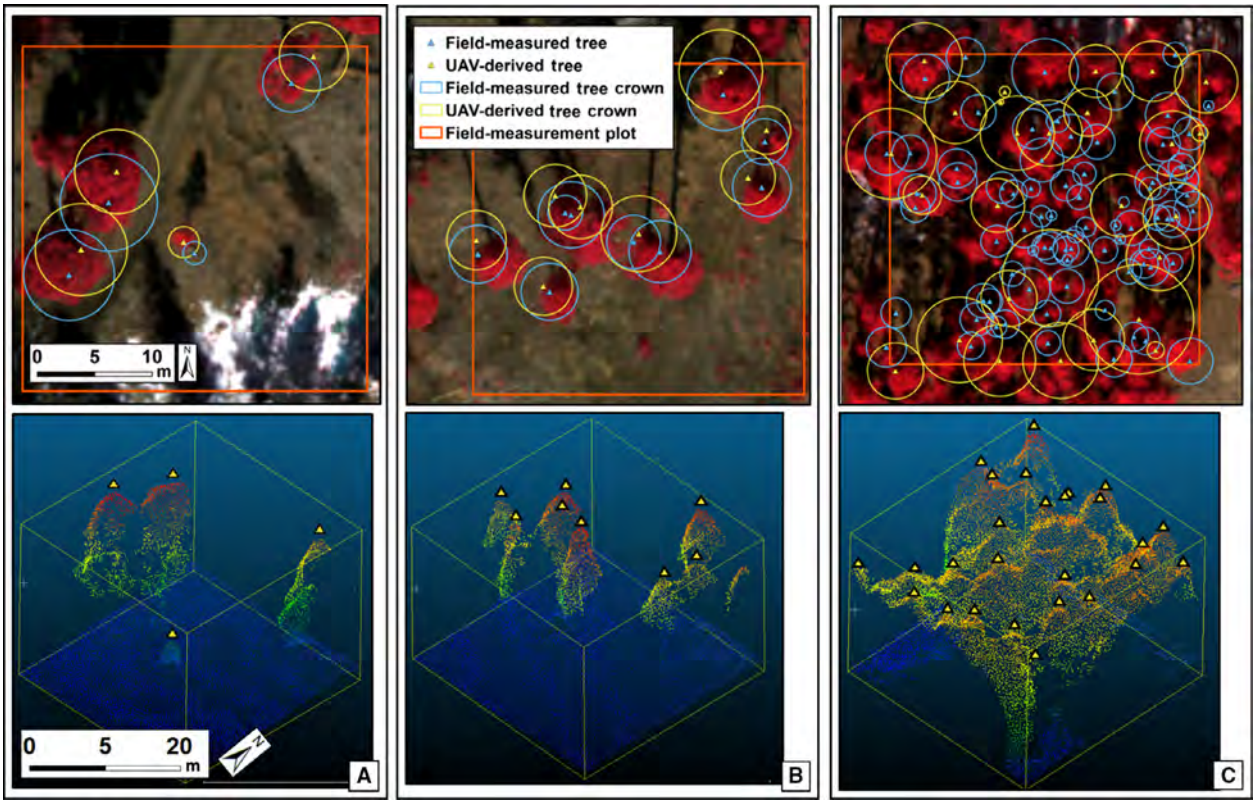

Figure 2. Examples of our field plots from each of the low- (A), medium- (B) and high- (C) density classes. The top row shows the UAV orthomosaic images overlaid with both the field-measured and UAV-derived tree locations as well as their corresponding crown diameters. The bottom row shows the Structure-from-Motion (SfM) point cloud data that corresponds to each plot above, as well as the SfM-derived tree locations placed on each respective tree.

Table 2. Individual tree omission and commission errors in the low-, medium- and high-density classes, with the overall scores across each density class provided. Analysis parameters included were the true positive (TP), false negative (FN), false positive (FP) trees, as well as the recall (*r*), precision (*p*) and F-score (*F*)

	Mean TPH	Mean CC (%)	Field-based measurement	UAV image-derived	TP	FN	FP	*r*	*p*	*F*
Low density (n = 7)	59	9	37	35	34	3	1	0.92	0.97	0.94
Medium density (n = 6)	139	17	75	57	53	22	4	0.71	0.93	0.8
High density (n = 4)	778	74	280	185	93	221	20	0.33	0.82	0.44

height and crown diameter estimates differed between density classes, with the low- and high-density classes consistently being the most and least accurate estimates, respectively (Table 3).

In the low-density class, 92% (n = 34) of the trees was correctly identified as True Positives (TP), with a recall (r) score of 0.92 (0.75–1.00), an overall precision (p) of 0.97 (0.86–1.00) and an F-Score of 0.94 (0.80–1.00) (Table 2). When we compared the location of these trees in the low-density class to the field-based GPS data, the mean difference in the coordinates' Euclidean distances was 2.44 m. A simple linear regression model comparing the field-based and UAV image-derived individual tree heights showed strong agreement with an adjusted R^2 = 0.95 (RMSE = 1.77 m) for these trees, while the regression model of the crown diameters showed moderate agreement with an adjusted R^2 = 0.61 (RMSE = 1.27 m).

In the medium-density class, 71% (n = 53) of the trees was correctly identified as true positives, with slightly lower recall (r = 0.71), precision (p = 0.93) and F-score values (F = 0.80) than for the low-density class (Table 2).

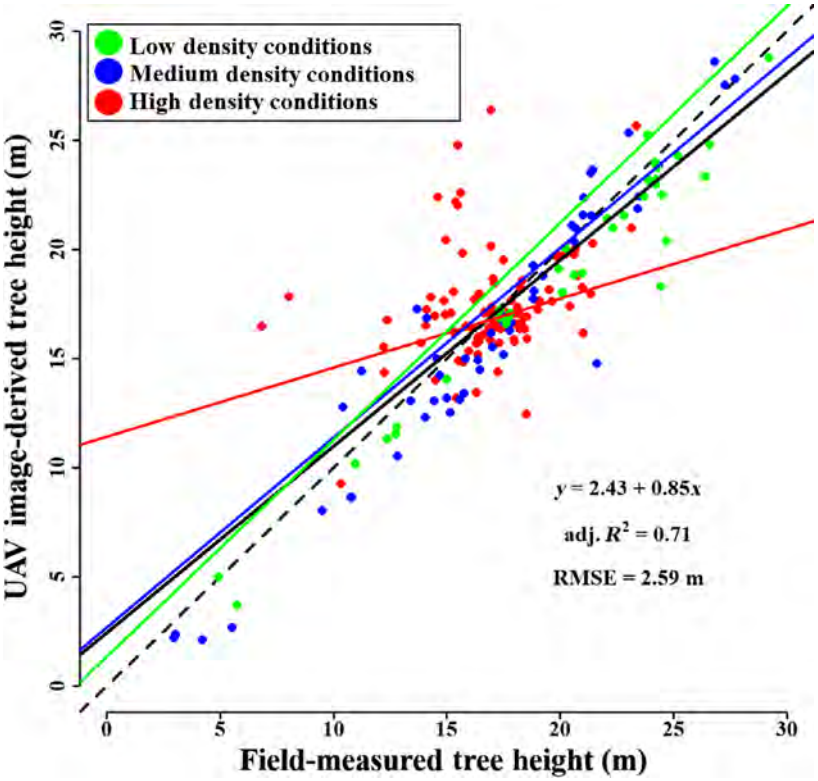

Figure 3. Linear regression models established between the field-measured and UAV image-derived individual tree height estimates. The dashed line is a 1:1 reference line and solid black line is the overall fitted regression model (adj. R^2 = 0.71). In addition, separate regression models were fit to each density class and the regression lines are colored accordingly.

Table 3. A summary of the UAV image-derived individual tree height and canopy diameter estimates, grouped by density classes, and compared to the US Forest Service Common Stand Exam (CSE) acceptable accuracy ranges. The reported values for each acceptable accuracy range indicate the percent of the total trees estimated from the UAV data within that range

	Tree height		Crown diameter	
	CSE ±10%	CSE ±20%	CSE ±10%	CSE ±20%
UAV image-derived estimates within CSE accuracy ranges				
Low density (n = 34)	85.3%	94.1%	26.5%	61.7%
Medium density (n = 53)	56.6%	84.9%	24.5%	41.5%
High density (n = 93)	58.0%	82.7%	4.3%	10.7%
Overall (n = 180)	62.7%	85.5%	14.4%	29.4%

The mean difference in the coordinates' Euclidean distances was lower than that of the low-density class at 1.92 m. The regression model of individual tree heights had an adjusted R^2 = 0.92 (RMSE = 1.87 m) (Fig. 3). The regression model of medium-density class crown diameters only had an adjusted R^2 = 0.09 (RMSE = 2.19 m).

In the high-density class, only 33% (n = 93) of the field-measured trees was correctly identified as true positives, with recall (r = 0.30), precision (p = 0.82) and F-score values (F = 0.44) lowest among the three density classes (Table 2). The lowest mean difference between the coordinates' Euclidean distances was observed for this density class at 1.54 m. The regression model of tree heights showed low agreement between the SfM-derived and field-measured heights with an adjusted R^2 = 0.08 (RMSE = 3.14 m) (Fig. 3), while the model comparing canopy diameters exhibited similar behavior with an adjusted R^2 = 0.005 (RMSE = 3.94 m).

Mid-scale forest structure metrics

Field-measured canopy cover and UAV image-derived estimates showed good agreement overall (adj. R^2 = 0.79; RMSE = 15.4%) (Fig. 4). When this agreement was assessed by density class, the medium-density relationship (adj. R^2 = 0.78; RMSE = 10.8%) was stronger than the low-(adj. R^2 = 0.72; RMSE = 10.7%) and high- (adj.

R^2 = 0.48; RMSE = 27.1%) density classes. ANOVA results indicated significant differences in UAV image-derived canopy cover estimates between the density classes ($F_{2,150}$ = 84.47, $P < 0.01$): the high-density class had significantly greater canopy cover than both the medium-($P < 0.01$) and low-($P < 0.01$) density classes. When we similarly assessed the UAV image-derived tree density estimates, there was a significant difference ($P = 0.03$) in TPH between the field-measured (M = 248.4 TPH; SD = 297.1 TPH) and UAV image-derived estimates (M = 129.4 TPH; SD = 107.6 TPH). Significant differences were also found between density classes in both the field-measured ($F_{2,14}$ = 106.9, $P < 0.01$) and UAV image-derived estimates ($F_{2,14}$ = 30, $P < 0.01$). The UAV image-derived TPH estimate in the high-density class was significantly greater than both the medium- ($P < 0.01$) and low- ($P < 0.01$) density classes.

Restoration treatment effects

When the UAV image-derived canopy cover estimates were compared across the treated portion of the study area from the pre-treatment and post-treatment dates, the results indicated that the restoration treatment reduced the forest canopy cover from 39.4% to 9.6%. Similarly, our results indicated that stem density was reduced from 212.4 TPH to 64.5 TPH and the corresponding basal area was reduced from 22.9 m²/ha to 13.2 m²/ha. Our patch and interspace analysis results indicated that the treatment created considerable canopy openings by breaking up once continuous forest patches, often leaving single trees or groups of 2–3 trees behind (Fig. 5). The restoration treatment increased the number of patches across the study site by 70.6%, while the mean patch area decreased by 80.8% to 0.13 ha (Table 4). The total patch area across the study site decreased by 39.6% with a corresponding 74% increase of interspace area. Measures of the average patch contiguity decreased overall, while both the average patch fractal dimension index value and the Euclidean nearest random point distance (ENRPD) increased. This indicates that the remaining patches are less contiguous to one another, have more complex shapes, and that there is more area between remaining patches, respectively (Table 4).

Next, we compared the UAV image-derived mid-scale forest structure metrics to the restoration treatment objectives stated in the forest restoration prescription (Table 5) to evaluate whether the objectives were achieved. Across the treated portion of the study area, the UAV image-derived estimates of BA showed a reduction from 22.9 m²/ha to 13.2 m²/ha, falling within the 11–14 m²/ha target range for the overall stand-level BA. Next, using a 5 m buffer along the stream course, we found that 138 trees were cut within this area. This reduction is more than the treatment objective, which emphasizes a retention of all stream course bank stabilization trees. The interspace areas, termed 'regeneration openings', cover roughly 9% of the study area, and range in size from 0.07 to 0.33 ha, which fell outside of the 15% total area as targeted, but within the 0.2–0.4 ha range targets. There was an average of 5.3 trees per 'regeneration' polygon remaining after treatment and the target range was 3–5 trees. Similarly, the restoration goals in the different tree group areas were met, with the remaining groups being more irregularly shaped and smaller in area. However, the average spacing between tree groups was found to be lower (5.35 m) than the target (12–18 m). Finally, the interspace tree density was found to be higher (9.5 TPH) than intended (2–5 TPH).

Discussion

Estimating fine-scale forest metrics

We used high-resolution UAV-derived multispectral imagery and SfM models to quantify fine-scale vertical and horizontal forest structure across a gradient of forest density conditions. We found that forest density played a significant role in the accuracy of individual tree detection, height and canopy diameter estimation. Across the field plots of all densities, the UAV image-derived data initially identified 46% of all individual trees and resulted in an overall accuracy of 60%. However, once parsed by density condition, the average accuracy increased to 92% in low-density plots and 71% for medium-density plots, but remained low at 33% for high-density plots. While other studies reported higher rates of overall true positive tree identification, even with plot-level density class distinctions (Guerra-Hernández et al. 2016; Mohan et al. 2017; Shin et al. 2018), the high-density plots used in our study were on average much denser (up to 778 TPH) than the high-density conditions (>300 TPH) considered elsewhere. We provide the first accuracy assessment of UAV image and SfM data in very high-density conditions and note that when stem density increases beyond approximately 500 TPH, UAV image-derived estimates cannot provide adequate accuracies.

The location of individual trees provided by the ITS was accurate overall, but was dependent on density conditions. Interestingly, the location accuracy improved as the density increased, with the mean error in tree coordinates for low-, medium- and high-density conditions at 2.44 m, 1.92 m and 1.54 m, respectively. We speculate that this is due to a combination of tree canopy size and complexity as well as the stem density. For example, the ITS algorithm identifies tree tops, but many tree canopies are

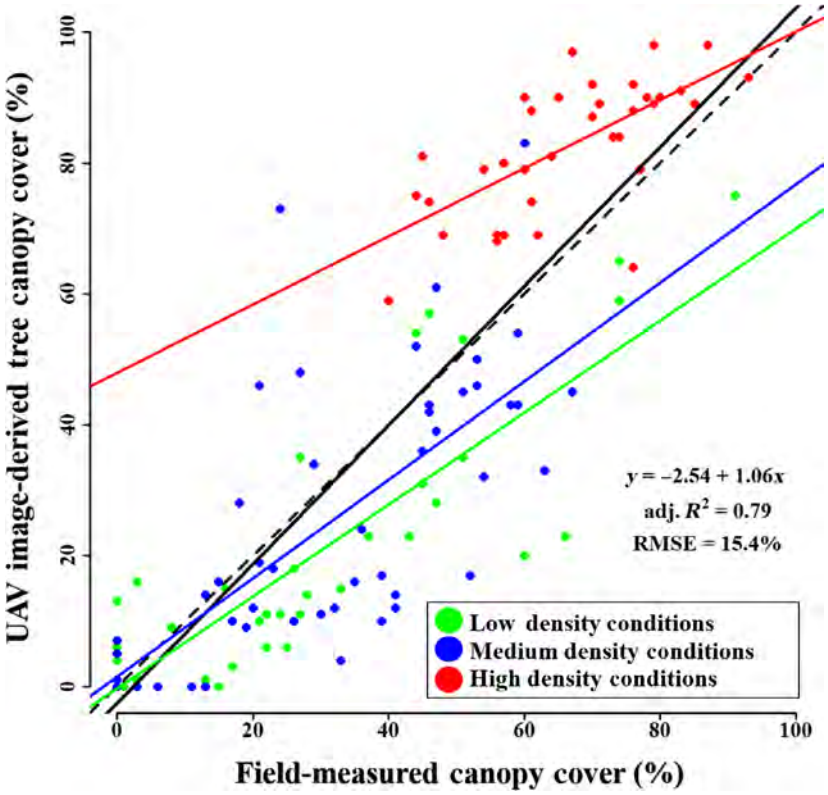

Figure 4. Linear regression models established between field-based measurements and UAV image-derived estimates of tree canopy cover. The dashed line is a 1:1 reference line and solid black line is the overall fitted regression model (adj. R^2 = 0.79). In addition, separate regression models were fit to each density class and the regression lines are colored accordingly. Data points here are the individual 10 m cells (n = 153) from the field-measured plots, which were summarized from the high-resolution (15 cm) binary canopy raster layers and are colored by density condition.

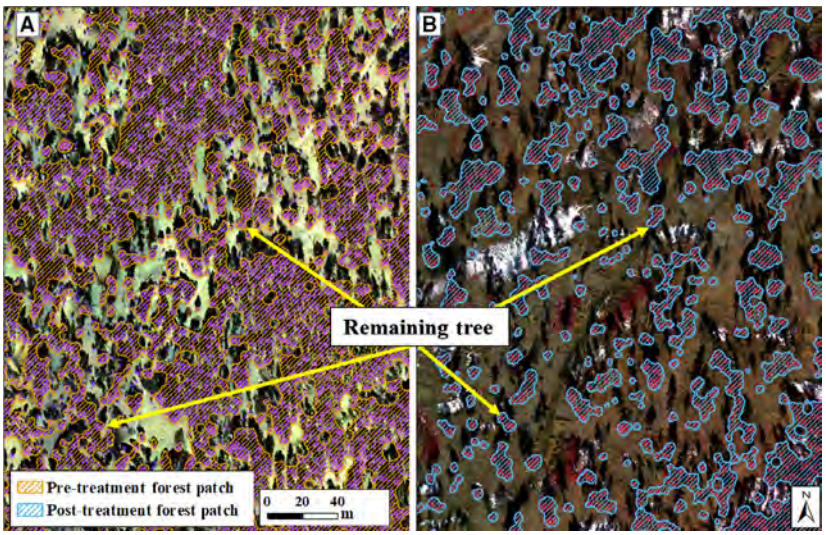

Figure 5. A comparison of pre-treatment (A) and post-treatment (B) forest patches illustrating substantial changes in horizontal structure and the creation of new forest patches. Toward the center of panel B, the vegetation not highlighted as a patch is fallen timber awaiting removal. The base map images are the respective UAV orthomosaic images in 15 cm resolution used for canopy cover and forest patch delineation.

Table 4. Patch and interspace metrics from the treated portion of the study area

	No. of patches	Total patch area (ha)	Total Interspace Area (ha)	Mean Patch Area (ha)	Patch Contiguity	Fractal Dimension Index	ENRPD (m)
Patch and interspace metrics							
Pre-Treatment	39	15.2	12.5	0.68	0.45 (range = 0.45)	1.12 (range = 0.41)	3.5 (range = 15.6)
Post-Treatment	133	5.9	21.8	0.13	0.41 (range = 0.60)	1.16 (range = 0.26)	7.1 (range = 38.9)

	No. of patches	Total patch area (ha)	Total interspace area (ha)	Mean patch area (ha)	Patch contiguity	ENRPD (m)
Patch and interspace metrics						
Pre-Treatment	39	15.2	12.5	0.68	0.45 (range = 0.45)	3.5 (range = 15.6)
Post-Treatment	133	5.9	21.8	0.13	0.41 (range = 0.60)	7.1 (range = 38.9)

Patch contiguity is a unitless metric, ranging from 0 to 1 where 0 is a single pixel patch and it approaches 1 as patch shape complexity and patch boundary configuration increase. Fractal dimension index is a unitless metric, ranging from 1 to 2 where 1 is a patch with a simple shape (e.g., square) and 2 is a patch with a more convoluted boundary. Euclidean nearest random point distance (ENRPD) is an assessment of the shortest straight-line distance between randomly generated points, and is used to measure the prevalence and size of forest gaps.

Table 5. A selection of the restoration treatment objectives outlined for the study area

Restoration treatment objective	Restoration treatment outcome
Final stand-level basal area (BA) = 11–14 m²/ha	Final BA = 13.2 m²/ha
Retain all stream course bank stabilization trees	Net loss of 138 trees
Regeneration openings should	
Be 15% of the treatment area	9% of treatment area
Range in size from 0.2 to 0.4 ha (up to 0.8 ha)	Range: 0.07–0.33 ha
Retain 3–5 reserve trees in openings larger than 0.4 ha	Average of 5.3 trees
Tree groups should	
Be irregularly shaped	Fractal dimension index = 1.16 (range 0.26)
Range in size from 0.04 to 0.4 ha (averaging 0.1–0.2 ha)	Range: 0.03–0.37 ha (mean 0.13 ha)
Distance b/t groups should be 12–18 m	Avg. distance = 5.35 m
Cut all remaining interspace trees, leaving 2–5 TPH	Density = 9.5 TPH

The restoration treatment outcomes were estimated from the post-treatment UAV image-derived datasets.

interlocked and tree tops are located closer together in high-density conditions. In comparison, trees in the lower density conditions are much farther apart leading to larger mean errors in their locations. They are also most often the largest trees with big canopy diameters because they were intentionally left uncut during the restoration treatment.

The UAV-derived individual tree height estimates performed well overall, with no significant differences between the UAV-derived and field-measured pairs. Furthermore, 86% of the individual tree height estimates were within the 20% acceptable error range of the USFS Common Stand Exam guidelines. The 86% accuracy is also well within the accepted rates of remotely sensed data analysis (Congalton and Green 2008). Taken together, these findings indicate that UAV image-derived methods can be used by forest restoration practitioners for estimating tree height. However, when parsed by density class, the relationships between the field-measured and UAV-image derived tree heights were notably different between both the low- and medium-density conditions versus the high-density conditions (Fig. 3). The results of the low- and medium-density conditions are consistent with findings of other research (Zarco-Tejada et al. 2014; Panagiotidis et al. 2016; Wallace et al. 2016) and might be due to the relatively high point densities present in the SfM point clouds. The lack of agreement in the high-density conditions appears to result from a combination of incorrectly identified tree tops, outlier points in the UAV dataset, and higher DTM error.

Individual tree crown diameters were not well estimated overall, with high-density conditions being the driver behind UAV-derived and field-measured differences. Overall, the agreement was poor except for in low-density conditions. Other studies have reported more accurate SfM-derived estimates of canopy diameter, but they included consistent tree spacing, higher spatial resolution data and less dense conditions (Zarco-Tejada et al. 2014; Díaz-Varela et al. 2015), none of which were present in this study. This underscores the notion that individual tree crown diameters, especially when measured using

UAV-image-based techniques, are subject to bias and error. Field techniques require a technician to visually determine a canopy dripline to estimate the canopy diameter. Since the UAV-image derived point cloud is often noisy yet continuous in high-density conditions, the canopy edges are obscured leading to inaccurate estimates of crown diameters. Other individual tree metrics such as crown bulk density and height to crown are of interest to regional forest managers due to their use in fire modeling and allometric equation development. However, since restoration practices occur at the mid- to landscape-scales, canopy cover is a more important metric and further improvements in its estimates are needed.

When compared to traditional USFS CSE accuracy standards, UAV image-derived tree crown diameters were within the ±10% and ±20% acceptable accuracy ranges for only 14% and 29% of the observations, respectively. Importantly, the high-density conditions again provided less accurate estimation for both tree height and crown diameter. This highlights the need to refine UAV image-derived estimates, especially for crown diameter, to ensure they provide a viable augmentation to CSE field measurement. This is especially important as UAV-borne remote sensing methods continue to be leveraged in forest mensuration and inventorying applications.

Estimating mid-scale forest metrics

When estimating mid-scale forest structure metrics, the UAV image-derived estimates of canopy cover, TPH and BA in high-density conditions were consistently significantly different from field-based estimates. In high-density conditions, canopy cover was consistently overestimated, while in low-density conditions it was underestimated (Fig. 4). We believe that this arises from the fact that our field methods employed two measurements of canopy diameter to calculate an average estimate for each tree canopy, while UAV-image derived estimates provide full coverage at 15 cm resolution pixels. Despite both methods being summarized to a plot-level estimate, we believe that the UAV-image derived data naturally provide a more complete and repeatable estimation overall. Using at-nadir images with NDVI estimates can eliminate potential bias between different field-based approaches (Fiala et al. 2006). Compared with the field-based measurements of TPH and BA, the UAV-based measurements underestimated these metrics in high-density conditions. As mentioned previously, the high-density conditions we measured were the highest observed thus far and allowed for a more realistic understanding of the limits of this methodology. Our observations in these conditions also highlight obvious areas of future improvement and demonstrate the UAV potential for restoration practitioners.

Restoration treatment outcomes

A central motivation of this study was to provide forest managers with a realistic evaluation of UAV image-derived estimates and workflows as a tool for assessing mechanical forest restoration treatments and their outcomes. As is the case for other regional restoration projects, the treatment at our study site relied on a set of prescriptive guidelines and desired outcomes (Table 5). We found that the treatment led to a 70% reduction in TPH, 42% reduction in BA and a 30% reduction in percent canopy cover. This increased the number of forest patches by 70%, where the average patch sizes are smaller in size with more complex shapes. Additionally, the total amount and complexity of forest patch interspace increased.

Restoration treatment outcomes showed an overall agreement with the restoration objectives. Five of the nine treatment goals that we assessed were successfully achieved (Table 5). We believe that these are strong results especially since the other restoration treatment objectives were still relatively close to their goal and displayed the overall intended trend. For example, scrutiny of the net loss of bank-stabilization trees, while counter to a specific treatment objective, revealed that the thinning operations favored shorter trees. Since the trees cut in these stream bank areas were shorter, they were likely considered undesirable according to a broader site-wide goal. We also found that the creation of 'regeneration opening' areas was not as extensive as the prescription had intended, but the size and shape of the remaining 'tree groups' were on target. It is important to note that the prescription we assessed was developed for the entire 138 ha treatment unit, of which we only assessed 30 ha. Objectives not met in this analysis could, therefore, be met if the entire treatment unit was assessed following implementation. In addition, variability in metrics across the treatment unit is desired. While potentially not met in one part of the unit, the average condition or range in conditions across the unit may be met, when the whole unit is assessed. Future studies might benefit from assessing a greater portion of the area corresponding to the prescription.

Other considerations for UAV applications

High-resolution multispectral UAV orthoimagery and SfM models offer an exciting new approach for forest inventorying and monitoring. As with any emerging technology, there are a number of specific shortcomings that we encountered which warrant attention. Similar to other studies, we found that environmental conditions (e.g., sun angle, wind, high ground reflectance), sensor resolution and flight plan characteristics all contributed to data

processing, the quality of final data products, and the derived tree structure estimates (Dandois et al. 2015; Iglhaut et al., 2019; Iizuka et al. 2018; Puliti et al. 2015). Perhaps most importantly, the nearly continuous canopy cover in higher-density forest conditions provides significant uncertainty. Specifically, we observed a final (dense) 3D point cloud with little variability in texture across the dense forest canopy and not enough ground points. This yields a DTM with relatively homogenous values and lower accuracies in high-density conditions (RMSE = 3.52), which influenced the overall accuracy (RMSE = 2.98 m) of the final DTM. In comparison, the accuracies observed in the low- and medium-density conditions were greater (RMSE = 2.21). This is consistent with previous studies and indicates that the ground surface occlusion under dense canopy degrades DTM accuracy (Dandois and Ellis 2010; Wallace et al. 2016) and subsequently impacts estimates of individual tree locations and heights (Dandois et al. 2015; Wallace et al. 2016; Mohan et al. 2017).

The homogenous DTM values also impacted tree segmentation, which underperformed in higher-density areas. Tree height and crown diameter estimates were subsequently affected by the segmentation issues and interlocking canopies. Thus, improving the DTM accuracy would likely provide a more heterogeneous canopy in dense conditions, leading to improved tree location, height and canopy diameter estimates. Using a more accurate DTM from an alternate source, such as an airborne lidar dataset, would presumably provide more accurate tree location and estimations, although these alternatives are often too coarse in spatial resolution, publically unavailable, or prohibitively expensive.

We experimented with varying parameters of the ITS algorithm, other ITS algorithms, as well as parsing the point cloud by density conditions. In the end, we decided that an overly complicated workflow might deter forest managers from adopting this methodology and applied the single best ITS algorithm and parameterization to the entire point cloud. We suggest that future attempts can improve ITS results and the subsequent tree height and crown diameter estimations by adopting lower flight altitudes, higher sensor resolution and by leveraging flight conditions with higher sun angles or overcast skies. These conclusions echo those of other similar work and underscore the importance of numerous data acquisition parameters on final product quality and accuracy (Dandois et al. 2015; Puliti et al. 2015). Our findings highlight that on-demand data acquisition, adaptable SfM workflows and a growing library of forest data-specific processing tools make UAV images a promising tool for estimating fine- and mid-scale forest structure metrics especially in low- and medium-density conditions.

As the need for forest restoration continues to increase, and the abilities of UAV-borne remote sensing are refined, the use of UAV-derived forest structure measurements has the potential to optimize restoration planning and monitoring. Restoration planning is often challenged with an accurate estimate of pre-treatment forest density conditions, which can now be rapidly acquired with a UAV. After an initial capital investment in UAV equipment and software of up to $30,000, data can be acquired and processed on demand which continually lowers long-term operation costs. When compared to the costs of traditional plot-level field surveys (~US$180 per plot), airborne lidar ($7.50–$6 per ha at 15,000–40,000 ha, respectively) or manned aerial imagery ($200,000–$500,000 over >10,000 ha), the costs associated with UAV-borne data acquisition are lower (Sankey et al. 2017). In our region, the pace, timing and implementation of restoration treatments are often dependent on weather and logging contractor availability. Having a flexible, standardized and cost-effective approach to assess and monitor restoration treatment outcomes can help forest managers operate more efficiently. Additionally, the mid-scale forest metrics and methodology we presented in this study can be applied to monitoring a wider array of forest restoration outcomes including wildfire risk and potential behavior, wildlife habitat characteristics and drought resilience components of a post-restoration landscape. Providing such assessments at high spatial and temporal resolution could enable restoration planning and adaptive management to occur at both a faster pace and greater scale.

Conclusions and Management Implications

UAV applications provide three unique advantages in monitoring forest restoration. First, forest managers can acquire data for individual treatments to tailor subsequent treatments and achieve larger landscape-scale benchmarks. Second, UAV data can be used to accurately quantify post-treatment conditions and compare them to prescription objectives. We found the most accurate fine- and mid-scale estimates of forest structure to occur across low-density conditions, which often correspond to post-treatment conditions. Third, pre- and post-treatment conditions can be directly compared for mid-scale forest metrics, especially canopy cover. Our findings support previous findings that demonstrated coarser (1 m pixel) resolution manned aerial digital photography can be used at the landscape scale (400 ha +) to assess canopy cover and forest patch and interspace characteristics. UAV image-derived mid-scale metrics can be leveraged for the high spatial and temporal resolution to provide nearly

continuous feedback to forest managers. Other study areas with understory shrub layers might also benefit from the high-resolution data that UAV sensors can provide, when classifying forest vegetation.

Future UAV-based research should focus on developing a spatially extensive sampling strategy to provide a more comprehensive evaluation of landscape-scale forest restoration. It is also important to include different treatment types and regionally relevant topographic and vegetative characteristics. This would allow for the detection of differences between varying prescriptions, allow for the workflow to be tailored to site-specific conditions, and better facilitate landscape-scale restoration monitoring.

Acknowledgement

Any use of trade, product, or firm names is for descriptive purposes only and does not imply endorsement by the U.S. Government.

References

Allen, C. D., M. Savage, D. A. Falk, K. F. Suckling, T. W. Swetnam, T. Schulke, et al. 2002. Ecological restoration of southwestern Ponderosa pine ecosystems: a broad perspective. *Ecol. Appl.* **12**, 1418–1433. https://doi.org/10.1890/1051-0761(2002)012[1418:erospp]2.0.co;2

Alonzo, M., H.-E. Anderse, D. Morton, and B. Cook.2018. Quantifying boreal forest structure and composition using UAV structure from motion. *Forests.* **9**, 119. https://doi.org/10.3390/f9030119.

Altschul, J. H., and H. C Fairley. 1989. Man, Models and management: an overview of the archaeology of the Arizona strip and the management of its cultural resources. https://doi.org/doi:10.6067/xcv8dv1m7h

Bohlin, J., I. Bohlin, J. Jonzén, and M. Nilsson. 2017. Mapping forest attributes using data from stereophotogrammetry of aerial images and field data from the national forest inventory. *Silva Fenn.* **51**, 1–8. https://doi.org/10.14214/sf.2021

Bottero, A., A. W. D'Amato, B. J. Palik, J. B. Bradford, S. Fraver, M. A. Battaglia, et al. 2017. Density-dependent vulnerability of forest ecosystems to drought. *J. Appl. Ecol.* **54**, 1605–1614. https://doi.org/10.1111/1365-2664.12847

Carr, J. C., and J. B. Slyder. 2018. Individual tree segmentation from a leaf-off photogrammetric point cloud. *Int. J. Remote Sens.* **39**, 5195–5210.

Castello, J. D., D. J. Leopold, and P. J. Smallidge. 2006. Pathogens, patterns, and processes in forest ecosystems. *Bioscience* **45**, 16–24. https://doi.org/10.2307/1312531

Congalton, R. G., and K. Green. 2008. *Assessing the accuracy of remotely sensed data: principles and practices*. Lewis Publishers, Bota Raton.

Cooper, C. F. 1960. Changes in vegetation, structure, and growth of southwestern pine forests since white settlement. *Ecol. Monogr.* **30**, 129–164. https://doi.org/10.2307/1948549

Cooper, C. F. 1961. Pattern in Ponderosa Pine forests. *Ecology* **42**, 493–499. https://doi.org/10.2307/1932235

Covington, W. W., and M. M. Moore.2006. Postsettlement changes in natural fire regimes and forest structure. *J. Sustain. Forest.* **2**, 153–181. https://doi.org/10.1300/j091v02n01_07.

Covington, W. W., P. Z. Fule, M. M. Moore, S. C. Hart, T. E. Kolb, J. N. Mast, et al. 1997. Restoring ecosystem health in Ponderosa pine forests of the southwest. *J. Forest.* **95**, 23–29.

Dahms, C. W., and B. W. Geils. 1997. An assessment of forest ecosystem health in the Southwest. Gen Technical Rep Rm-Gtr-295 Fort Collins Co U S Dep Agriculture Forest Service Rocky Mountain Forest Range Experimental Station 97 P, 295. https://doi.org/10.2737/rm-gtr-295

Dandois, J. P., and E. C. Ellis. 2010. Remote sensing of vegetation structure using computer vision. *Remote Sens.* **2**, 1157–1176. https://doi.org/10.3390/rs2041157

Dandois, J. P., and E. C. Ellis. 2013. High spatial resolution three-dimensional mapping of vegetation spectral dynamics using computer vision. *Remote Sens. Environ.* **136**, 259–276. https://doi.org/10.1016/j.rse.2013.04.005

Dandois, J. P., M. Olano, and E. C. Ellis. 2015. Optimal altitude, overlap, and weather conditions for computer vision uav estimates of forest structure. *Remote Sens.* **7**, 13895–13920. https://doi.org/10.3390/rs71013895

Day, K., J. Berg, H. Brown, T. Crow, J. Morrison, G. Nowacki, et al. 2006. Ecosystem restoration: a framework for restoring and maintaining the national forests and grasslands. Retrieved from https://www.fs.fed.us/restoration/documents/RestFramework_final_010606.pdf

Diaz-Varela, R., E. Gonzalez-Ferreiro, A. C. Correia, A. Nunes, M. Tomé, J. Guerra-Hernandez, et al. 2016. Using high resolution UAV imagery to estimate tree variables in *Pinus pinea* plantation in Portugal. *Forest Syst.* **25**, eSC09. https://doi.org/10.5424/fs/2016252-08895

Díaz-Varela, R. A., R. de la Rosa, L. León, and P. Zarco-Tejada. 2015. High-resolution airborne UAV imagery to assess olive tree crown parameters using 3D photo reconstruction: application in breeding trials. *Remote Sens.* **7040421**:4213–4232. https://doi.org/10.3390/rs70404213

Dieterich, J. H. 1980. *Chimney Springs forest fire history*. USDA Forest Service Research Paper RM-220, Fort Collins, CO.

FAO (Food and Agriculture Organization of the United Nations). 2015. Global Forest Resources Assessment 2015. Retrieved from http://www.fao.org/3/a-i4808e.pdf

Fiala, A. C. S., S. L. Garman, and A. N. Gray. 2006. Comparison of five canopy cover estimation techniques in the western Oregon Cascades. *For. Ecol. Manage.* **232**, 188–197. https://doi.org/10.1016/j.foreco.2006.05.069

Fitch, R. A., Y. S. Kim, A. E. M. Waltz, and J. E. Crouse. 2018. Changes in potential wildland fire suppression costs due to

restoration treatments in Northern Arizona Ponderosa pine forests. *For. Policy Econ.* **87**, 101–114. https://doi.org/10.1016/j.forpol.2017.11.006

Fitzgerald, S. A. 2005. Fire ecology of ponderosa pine and the rebuilding of fire-resilient ponderosa pine. *USDA Forest Service General Technical Report*, *97756*, PSW-GTR-198.

Four Forests Restoration Initiative. 2013. (4FRI) Adaptive management, biophysical and socio-economic monitoring plan December 2013.

Fulé, P. Z. 2008. Does it make sense to restore wildland fire in changing climate? *Restor. Ecol.* **16**, 526–532. https://doi.org/10.1111/j.1526-100X.2008.00489.x

Fulé, P. Z., W. W. Covington, and M. M. Moore. 1997. Determining reference conditions for ecosystem management of southwestern Ponderosa pine forests. *Ecol. Appl.* **7**, 895–908. https://doi.org/10.1890/1051-0761(1997)007[0895:drcfem]2.0.co;2

Fulé, P. Z., J. E. Crouse, A. E. Cocke, M. M. Moore, and W. W. Covington. 2004. Changes in canopy fuels and potential fire behavior 1880-2040: grand Canyon, Arizona. *Ecol. Model.* **175**, 231–248. https://doi.org/10.1016/j.ecolmodel.2003.10.023

Girvetz, E. H., and S. E. Greco. 2007. How to define a patch: a spatial model for hierarchically delineating organism-specific habitat patches. *Landscape Ecol.* **22**, 1131–1142. https://doi.org/10.1007/s10980-007-9104-8

Guerra-Hernández, J., E. González-Ferreiro, A. Sarmento, J. Silva, A. Nunes, A. C. Correia, et al. 2016. Using high resolution UAV imagery to estimate tree variables in *Pinus pinea* plantation in Portugal. *Forest Syst.* **25**, 9. https://doi.org/10.5424/fs/2016252-08895

Hudak, A., A. M. Smith, J. G. Evans, M. J. Falkowski, and M. J. 2006. Estimating coniferous forest canopy cover from LiDAR and multispectral data. *American Geophysical Union, Fall Meeting 2006*.

Huffman, D. W., M. M. Moore, W. W. Covington, J. E. Crouse, and P. Z. Fulé. 2001. Ponderosa pine forest reconstruction: comparisons with historical data. *Ponderosa Pine Ecosystems Restoration and Conservation: Steps Towards Stewardship*, 3–8.

Iglhaut, J., C. Cabo, S. Puliti, L. Piermattei, J. O'Connor, and J. Rosette.2019. Structure from Motion Photogrammetry in Forestry: a Review. *Curr. Forest. Rep.* **5**, 155. https://doi.org/10.1007/s40725-019-00094-3.

Iizuka, K., T. Yonehara, M. Itoh, and Y. Kosugi. 2018. Estimating tree height and Diameter at Breast Height (DBH) from Digital surface models and orthophotos obtained with an unmanned aerial system for a Japanese Cypress (*Chamaecyparis obtusa*) forest. *Remote Sens.* **10**, 13. https://doi.org/10.3390/rs10010013

Kalies, E. L., and S. S. Rosenstock. 2013. Stand structure and breeding birds: implications for restoring ponderosa pine forests. *J. Wildl. Manage.* **77**, 1157–1165. https://doi.org/10.1002/jwmg.577

Kolb, T. E., M. R. Wagner, and W. W. Covington. 1994. Concepts of forest health: utilitarian and ecosystem perspectives. *J. Forest.* **92**, 10–15 Retrieved from http://scholarsarchive.library.oregonstate.edu/xmlui/handle/1957/17277

Landres, P. B., P. Morgan, and F. J. Swanson. 1999. Overview of the use of natural variability concepts in managing ecological systems. *Ecol. Appl.* **9**, 1179–1188.

Larson, A. J., and D. Churchill. 2012. Tree spatial patterns in fire-frequent forests of western North America, including mechanisms of pattern formation and implications for designing fuel reduction and restoration treatments. *For. Ecol. Manage.* **267**, 74–92. https://doi.org/10.1016/j.foreco.2011.11.038

Li, W., Q. Guo, M. Jakubowski, and M. Kelly.2012. A new method for segmenting individual trees from the lidar point cloud. *Photogramm. Eng. Remote Sensing* **78**, 75–84.

Mast, J., P. Z. Fulé, M. M. Moore, W. W. Covington, and A. E. M. Waltz. 1999. Restoration of presettlement age structure of an Arizona Ponderosa pine forest. *Ecol. Appl.* **9**, 228–239. https://doi.org/10.1890/1051-0761(1999)009[0228:ropaso]2.0.co;2

Matonis, M. S., and D. Binkley. 2018. Not just about the trees: key role of mosaic-meadows in restoration of Ponderosa pine ecosystems. *For. Ecol. Manage.***411**, 120–131. https://doi.org/10.1016/j.foreco.2018.01.019

McGarigal, K., S. A. Cushman, and E. Ene. 2012. *FRAGSTATS v4: spatial pattern analysis program for categorical and continuous maps*. Amherst, MA.

Mohan, M., C. Silva, C. Klauberg, P. Jat, G. Catts, A. Cardil, et al. 2017. Individual tree detection from Unmanned Aerial Vehicle (UAV) derived canopy height model in an open canopy mixed Conifer Forest. *Forests* **8**, 340. https://doi.org/10.3390/f8090340

Moore, M. M., D. W. Huffman, P. Z. Fulé, W. Wallace Covington, and J. E. Crouse. 2004. Comparison of historical and contemporary forest structure and southwestern Ponderosa pine forests. *For. Sci.* **50**, 162–176.

Næsset, E. 2004. Practical large-scale forest stand inventory using a small-footprint airborne scanning laser. *Scand. J. For. Res.* **19**, 164–179. https://doi.org/10.1080/02827580310019257

Panagiotidis, D., A. Abdollahnejad, P. Surový, and V. Chiteculo. 2016. Determining tree height and crown diameter from high-resolution (UAV) imagery. *Int. J. Remote Sens.* **38**, 2392–2410. https://doi.org/10.1080/01431161.2016.1264028

Patton, D. R. 1977. Managing southwestern ponderosa pine for the Abert squirrel. *J. Forest.* **75**, 264–267.

Pearson, G. A. 1923. Natural reproduction of western yellow pine in the Southwest. In *Bulletin of the U.S Department of Agriculture; no.1105*.https://doi.org/10.5962/bhl.title.64666

Pelz, K., and Y. Dickinson. 2014. Monitoring forest cover spatial patterns with aerial imagery: A tutorial. Technical Brief CFRI-TB-1401, p. 50. Colorado State University.

Puliti, S., H. O. Ørka, T. Gobakken, and E. Næsset. 2015. Inventory of small forest areas using an unmanned aerial system. *Remote Sens.* **7**, 9632–9654. https://doi.org/10.3390/rs70809632

Reutebuch, S. E., H.-E. Andersen, and R. J. McGaughey. 2005. Light Detection and Ranging (LIDAR): an Emerging Tool for Multiple Resource Inventory. *J. Forest.* **103**, 286–292 Retrieved fromhttps://academic.oup.com/jof/article-abstract/103/6/286/4598654

Reynolds, R. T., A. J. S. Meador, J. A. Youtz, T. Nicolet, M. S. Matonis, P. L. Jackson, et al. 2013. Restoring composition and structure in southwestern frequent-fire forests. *USDA Forest Service*, *RMRS-GTR-3*.

Roussel, J.-R., J. Caspersen, M. Béland, S. Thomas, and A. Achim. 2017. Removing bias from LiDAR-based estimates of canopy height: accounting for the effects of pulse density and footprint size. *Remote Sens. Environ.* **198**, 1–16. https://doi.org/10.1016/J.RSE.2017.05.032

Rupnik, E., M. Daakir, and M. Pierrot Deseilligny. 2017. MicMac – a free, open-source solution for photogrammetry. *Open Geospatial Data Softw. Stand.* **2**, 14. https://doi.org/10.1186/s40965-017-0027-2

Sackett, S. S. 1979. *Natural fuel loadings in ponderosa pine and mixed conifer forests of the southwest*. USDA Forest Service Research Paper RM-213, Fort Collins, CO.

Sánchez Meador, A. J., and M. M. Moore. 2011. Reprint of: lessons from long-term studies of harvest methods in southwestern ponderosa pine–Gambel oak forests on the Fort Valley Experimental Forest, Arizona, USA. *For. Ecol. Manage.* **261**:923–936. https://doi.org/10.1016/j.foreco.2010.11.010

Sankey, T., J. Donager, J. McVay, and J. B. Sankey. 2017. UAV lidar and hyperspectral fusion for forest monitoring in the southwestern USA. *Remote Sens. Environ.* **195**, 30–43. https://doi.org/10.1016/j.rse.2017.04.007

Sankey, T., J. Leonard, and M. Moore.2019. Unmanned aerial vehicle – Based rangeland monitoring: examining a century of vegetation changes. *Rangel. Ecol. Manag.* **72**, 858–863.

Schubert, G. H. 1974. Silviculture of southwestern ponderosa pine: the status of our knowledge. Retrieved from https://www.fs.usda.gov/treesearch/pubs/35043

Schultz, C. A., T. Jedd, and R. D. Beam. 2012. The collaborative forest landscape restoration program: a history and overview of the first projects. *J. Forest.* **110**, 381–391. https://doi.org/10.5849/jof.11-082

Schultz, C. A., D. L. Coelho, and R. D. Beam. 2014. Design and governance of multiparty monitoring under the (USDA) forest service's collaborative forest landscape restoration program. *J. Forest.* **112**, 198–206. https://doi.org/10.5849/jof.13-070

Shin, P., T. Sankey, M. M. Moore, and A. E. Thode. 2018. Evaluating unmanned aerial vehicle images for estimating forest canopy fuels in a ponderosa pine stand. *Remote Sens.* **10**, 1266. https://doi.org/10.3390/rs10081266

Smith, W. B. 2002. Forest inventory and analysis: a national inventory and monitoring program. *Environ. Pollut.* **116** (SUPPL. 1), S233–S242. https://doi.org/10.1016/S0269-7491(01)00255-X

Snavely, N., S. M. Seitz, and R. Szeliski. 2006. Photo tourism. *ACM. T Graphic.***25**. https://doi.org/10.1145/1141911.1141964

Swetnam, T. W., and J. L. Betancourt. 2010. Mesoscale disturbance and ecological response to decadal climatic variability in the American Southwest. Pp. 329–359 *in* M. Stoffel, M. Bollschweiler, D. R. Butler and B. H. Luckman, eds. *Advances in global change research* (vol. **41**). Springer, Dordrecht. https://doi.org/10.1007/978-90-481-8736-2_32

Swetnam, T. W., C. D. Allen, and J. L. Betancourt. 1999. Applied historical ecology: using the past to manage for the future. *Ecol. Appl.* **9**:1120–1189.

Thiel, C., and C. Schmullius. 2016. Comparison of (UAV) photograph-based and airborne lidar-based point clouds over forest from a forestry application perspective. *Int. J. Remote Sens.* **38**, 1–16. https://doi.org/10.1080/01431161.2016.1225181

USGS. 2017. Unmanned aircraft systems data post-processing. In USGS National UAS Project Office. Retrieved from https://www.faa.gov/uas/

Wallace, L., A. Lucieer, Z. Malenovský, D. Turner, and P. Vopěnka. 2016. Assessment of forest structure using two UAV techniques: a comparison of airborne laser scanning and structure from motion SfM point clouds. *Forests* **7**, 62. https://doi.org/10.3390/f7030062

Weldon, L. 2014. Ecological restoration in the United States. Speech Presented at Ecosystems, Economy, and Society. Retrieved from https://www.fs.fed.us/speeches/ecological-restoration-united-states

White, A. S. 1985. Presettlement regeneration patterns in a southwestern ponderosa pine stand. *Ecology* **66**, 589–594. https://doi.org/10.2307/1940407

White, J. C., M. A. Wulder, M. Vastaranta, N. C. Coops, D. Pitt, and M. Woods. 2013. The utility of image-based point clouds for forest inventory: a comparison with airborne laser scanning. *Forests* **4**, 518–536. https://doi.org/10.3390/f4030518

Williamson, M., S. Rosenstock, and L. Kalies. 2011. Four forest restoration initiative: stakeholders' initial science needs assessment. {4FRI} Science and Monitoring Working Group.

Woolsey, T. S. 1911. Western yellow pine in Arizona and New Mexico. Retrieved from https://www.fs.usda.gov/treesearch/pubs/37531

Zarco-Tejada, P. J., R. Diaz-Varela, V. Angileri, and P. Loudjani. 2014. Tree height quantification using very high resolution imagery acquired from an unmanned aerial vehicle (UAV) and automatic 3D photo-reconstruction methods. *Eur. J. Agron.* **55**, 89–99. https://doi.org/10.1016/j.eja.2014.01.004

Zhang, W., J. Qi, P. Wan, H. Wang, D. Xie, X. Wang, et al.2016. An easy-to-use airborne LiDAR data filtering method based on cloth simulation. *Remote Sens.* **8**, 501.

